PAPER

Insight into heterogeneous dynamics of growing islands using coherent x-ray scattering

I Dax[1], I A Zaluzhnyy[1,*] ©, A Pylypenko[1], N Russegger[1], V Starostin[1] ©, R Rysov[2] ©, F Westermeier[2] ©, M Sprung[2], A Hinderhofer[1], L Pithan[1,3] © and F Schreiber[1,*] ©

[1] Institut für Angewandte Physik, Universität Tübingen, 72076 Tübingen, Germany
[2] Deutsches Elektronen-Synchrotron DESY, Notkestraße 85, 22607 Hamburg, Germany
[3] Present address: Deutsches Elektronen-Synchrotron DESY, Notkestraße 85, 22607 Hamburg, Germany.
[*] Authors to whom any correspondence should be addressed.

E-mail: ivan.zaluzhnyy@uni-tuebingen.de and frank.schreiber@uni-tuebingen.de
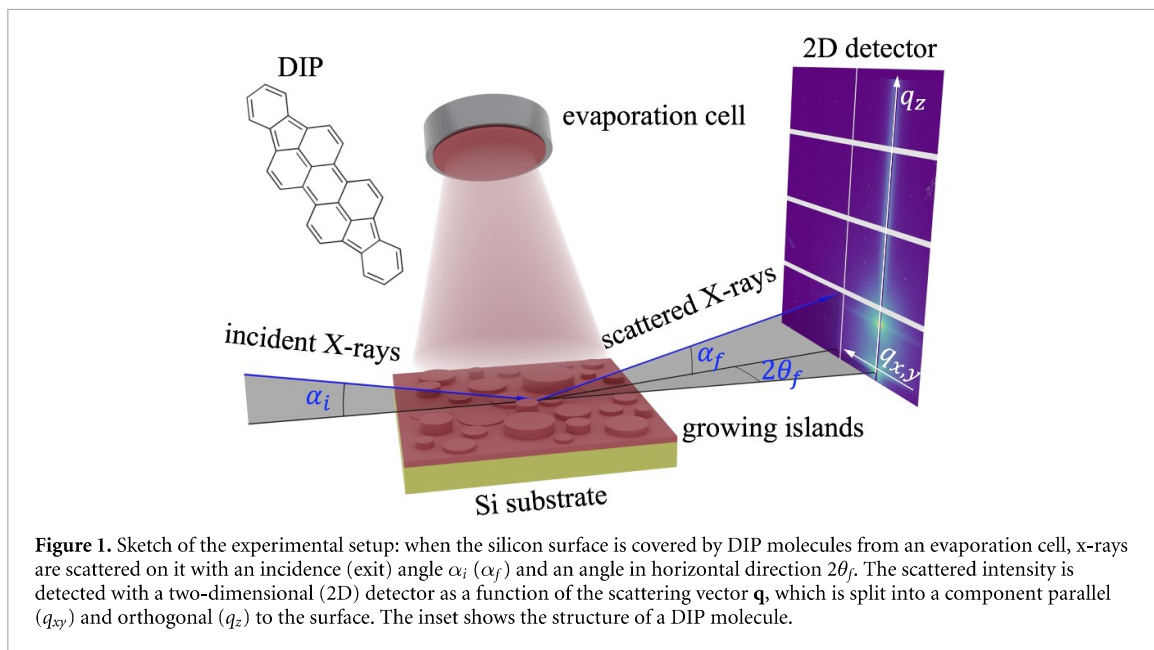
Abstract

Understanding the non-equilibrium structure formation of thin films is a fundamental challenge with important implications also for technical applications. The interplay between adsorption, desorption, and surface diffusion may result in the formation of nontrivial surface morphologies. X-ray photon correlation spectroscopy opens up new possibilities for understanding these processes. In this work, we perform *in situ* x-ray experiments in grazing incidence geometry to follow the growth of diindenoperylene thin films in real time, revealing details of the dynamics during molecular island formation. Comparison with simulations allows to extract dynamic and kinetic time scales. We observe time scales in the range of a few hundred seconds which occur mainly due to kinetics, i.e. island growth. Importantly, we can relate the observed heterogeneous behavior in dynamics to the number of open layers, revealing information about the change in the roughness, and the growth speed of each layer.

1. Introduction

Thin films are among of the most ubiquitous structures in modern technology. Fundamentally, the growth of thin films is a classical example of a statistical non-equilibrium process [1], where the resulting morphology, structure, and hence the properties of the film depend on the underlying dynamics and kinetics [2]. This causes the need not only to perform post-growth characterization of the films, but also study the growth process *in situ*. X-ray diffraction has been traditionally used for such studies [3] due to its non-destructive nature and ease of integration into growth setups. However, conventional x-ray scattering typically provides only averaged information about the film's structure and morphology.

Recent improvements of synchrotron sources enable the application of novel coherent scattering techniques based on x-ray photon correlation spectroscopy (XPCS) [4–9], which offer additional insights into thin film growth and can be also applied *in situ* [10, 11]. These techniques can provide an unprecedented level of detail about the arrangement of the surface during the growth process, including the adsorption of molecules on the substrate and the subsequent formation, realignment and diffusion of molecular islands.

Building upon these advances, here we demonstrate the quantification of the heterogeneity of growth dynamics. Specifically, we study the growth of diindenoperylene (DIP) on silicon, which is a prototypic organic semiconductor. Importantly, the conventional (i.e. non-XPCS) characterization has already been performed, serving as a detailed reference base [12–14]. In recent years, interest in organic materials has increased due to their ease of processing, low cost, and flexibility. However, the anisotropy of organic molecules in these films introduces an additional orientational degree of freedom and anisotropic interactions [12–19], affecting the structure and properties of the film. As a result, complex growth scenarios can occur in which initial monolayers (MLs) can fully close, or rapidly start to roughen along with unusual

Figure 1. Sketch of the experimental setup: when the silicon surface is covered by DIP molecules from an evaporation cell, x-rays are scattered on it with an incidence (exit) angle α_i (α_f) and an angle in horizontal direction $2\theta_f$. The scattered intensity is detected with a two-dimensional (2D) detector as a function of the scattering vector **q**, which is split into a component parallel (q_{xy}) and orthogonal (q_z) to the surface. The inset shows the structure of a DIP molecule.

growth behavior—depending on external conditions such as growth rate or substrate temperature [12, 13, 15].

By comparing experimental measurements to simulated data, we quantify the dynamics of the growth process. The results indicate that the prominent intensity fluctuations on the time scale of $\sim$100 s are dominated by kinetic effects, suggesting a stationary evolution of the islands. We further demonstrate how heterogeneous dynamics directly relate to the evolution of MLs, providing estimates for the roughness and time scales for the coverage of incomplete MLs.
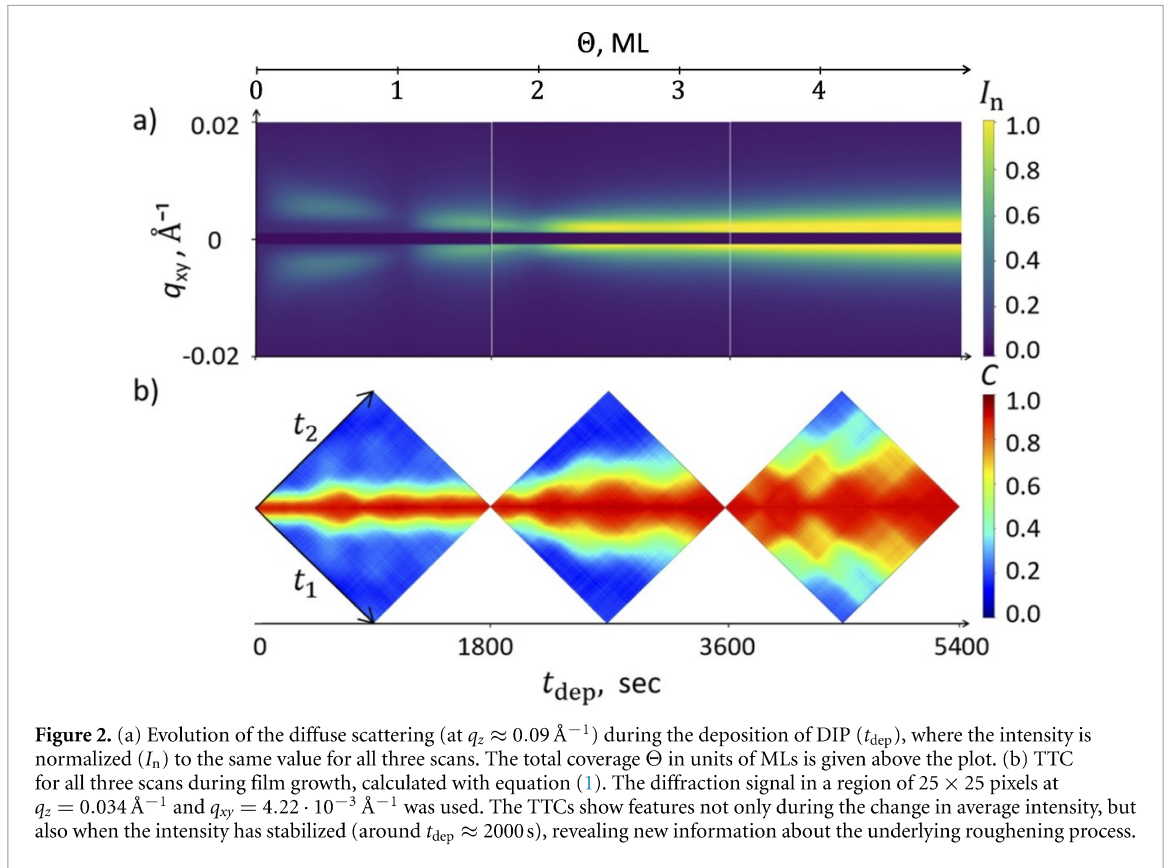
2. Experiment

We investigate the growth of DIP films during organic molecular beam deposition [14, 15, 20] on silicon substrates at a slightly elevated temperature ($T_{\text{sub}} \approx 40\,^{\circ}\text{C}$). The films were grown in our portable ultra-high vacuum chamber [21] at a rate of 0.1 nm min^{-1} until a final thickness of about 10 nm was reached.

The experiment was performed at the Coherence Applications Beamline P10 at PETRA III (DESY, Hamburg) using an x-ray beam focused to $8\,\mu\text{m} \times 5\,\mu\text{m}$ (hor. $\times$ vert.) with a photon energy of $E = 8.7\,\text{keV}$. To resolve the speckles in the scattered x-ray intensity, a two-dimensional (2D) detector (Eiger X 4M, pixel size $75\,\mu\text{m} \times 75\,\mu\text{m}$) was placed 5 meters downstream from the sample (figure 1). To ensure sensitivity regarding the surface changes and suppress contributions from the substrate, we performed the measurements in grazing incidence small angle x-ray scattering geometry [5, 22]. We thus choose an incidence angle of $\alpha_i = 0.15^{\circ}$, which is slightly below the critical angle of DIP ($\alpha_c = 0.17^{\circ}$) at the given x-ray energy [22]. To prevent radiation damage to the DIP film, we split the growth run into three scans of 1800 s each and changed the x-ray spot on the film between the scans. During one scan, we collected diffraction patterns every two seconds with 1 s of exposure time and 1 s of waiting time.

3. Experimental results

It is known that at room temperature the DIP film exhibits a near layer-by-layer growth for the first few layers, and then the formation of molecular islands leads to a so-called rapid roughening [12, 13, 15]. To separate these two different regimes of the film growth, we analyzed the diffuse scattering well above the critical angle, at $q_z \approx 0.09\,\text{Å}^{-1}$ (figure 2(a)). The intensity of the diffuse scattering is related to the roughness of the film surface. The absence of diffuse scattering indicates that all molecular layers are closed and there are no molecular islands on the film [10, 23]. Figure 2(a) shows that the first two layers open and close completely, afterwards the surface becomes rough (for better orientation during the growth process, the total coverage Θ in units of monolayers (ML) is given above the plot, the thickness of one layer is expected to be 1.6 nm [12]). Additionally, the maximum of diffuse scattering shifts to smaller values of q_{xy} during the film growth, indicating that the surface correlation length increases until it stabilises, starting from the third layer

Figure 2. (a) Evolution of the diffuse scattering (at $q_z \approx 0.09\,\text{Å}^{-1}$) during the deposition of DIP (t_{dep}), where the intensity is normalized (I_{n}) to the same value for all three scans. The total coverage Θ in units of MLs is given above the plot. (b) TTC for all three scans during film growth, calculated with equation (1). The diffraction signal in a region of 25×25 pixels at $q_z = 0.034\,\text{Å}^{-1}$ and $q_{xy} = 4.22 \cdot 10^{-3}\,\text{Å}^{-1}$ was used. The TTCs show features not only during the change in average intensity, but also when the intensity has stabilized (around $t_{\text{dep}} \approx 2000\,\text{s}$), revealing new information about the underlying roughening process.

at $l_{\text{corr}} \propto 2\pi/q_{xy} \approx 450\,\text{nm}$. This length scale corresponds to the average in-plane size of the surface roughness [24] and can be interpreted as a typical size of molecular islands that are formed during film growth.

The XPCS analysis of the film growth is based on the two-time correlation (TTC) calculated according to [25]

$$C\left(\mathbf{q}, t_1, t_2\right) = \frac{\left\langle\left(I_1 - \bar{I}_1\right)\left(I_2 - \bar{I}_2\right)\right\rangle}{\sqrt{\left\langle\left(I_1 - \bar{I}_1\right)^2\right\rangle} \cdot \sqrt{\left\langle\left(I_2 - \bar{I}_2\right)^2\right\rangle}}, \tag{1}$$
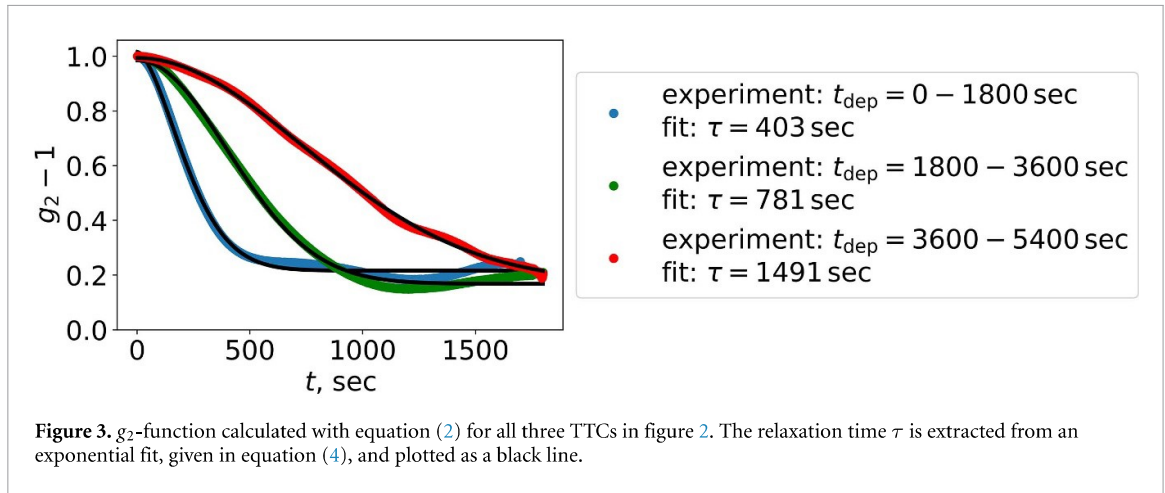
where $I_{1,2} \equiv I(t_{1,2}, \mathbf{q})$, $\mathbf{q}$ is the scattering vector, $\bar{I}_{1,2} \equiv \langle I_{1,2}\rangle$, and the averaging $\langle\ldots\rangle$ is performed over the pixels in the selected region of interest of the 2D diffraction pattern. Here, we used the diffraction signal in a region of 25×25 pixels at $q_z = 0.034\,\text{Å}^{-1}$ and $q_{xy} = 4.22 \cdot 10^{-3}\,\text{Å}^{-1}$, where the intensity of diffuse scattering was high enough to obtain reliable results. The selected q-range corresponds to the length scales of $l_z \approx 15\,\text{nm}$ and $l_{xy} \approx 150\,\text{nm}$ in real space, so the changes in the XPCS signal can be associated with the motion of molecular islands.

The experimental TTCs are shown in figure 2(b) in dependence of the deposition time $t_{\text{dep}} = (t_1 + t_2)/2$. The broadening perpendicular to the diagonal (i.e. with increase of t_{dep}) indicates an overall slowdown during growth. In addition, we see some 'irregularities' along the diagonal (successive slowing down followed by acceleration, i.e. non-monotonic behavior) which are usually referred to as dynamical heterogeneity [5, 6, 26]. These features may be caused to some extent by the layer closing and opening [10] for the growth times $t_{\text{dep}} \leqslant 2600\,\text{s}$, but they also appear at later stages, when no layer closing is happening anymore. Thus, if we focus on the intensity after $t_{\text{dep}} \approx 2000\,\text{s}$, the average intensity is not revealing more valuable information, as it remains constant. Nevertheless, the TTCs continue to show intriguing patterns. Accordingly, the exploration of this hidden insight into the roughening process can only be investigated with the use of XPCS.

4. Extraction of relaxation rates

Despite the fact that film growth is a nonequilibrium process, one can still estimate characteristic time scales by an analysis of the g_2-function [6, 10]

$$g_2\left(\mathbf{q}, t\right) - 1 = \left\langle C\left(\mathbf{q}, t_1, t\right)\right\rangle_{t_1} \tag{2}$$

Figure 3. g_2-function calculated with equation (2) for all three TTCs in figure 2. The relaxation time τ is extracted from an exponential fit, given in equation (4), and plotted as a black line.

with the time difference

$$t = |t_2 - t_1|. \tag{3}$$

The resulting g_2 curves obtained from the three TTC functions (figure 2(b)) are shown in figure 3. The non-monotonic decay of the g_2-function arises from the heterogeneous behavior of the TTC, which will be considered in section 6. At this stage, we can still derive averaged physical quantities using exponential fits, according to [4–6]

$$g_2\left(\mathbf{q}, t\right) - 1 = b + a \cdot \exp\left(-2 \cdot \left(\frac{t}{\tau}\right)^{\gamma}\right), \tag{4}$$

with the relaxation time τ, revealing the time scale of the underlying physical process. Additionally, a background b and a magnitude a are included to account for the finite contrast of the experimental data. Furthermore, the stretching exponent γ is introduced into the fit to take into account non-Brownian dynamics of the islands. The results of these fits, in particular the values of τ, are shown in figure 3. Our first conclusion is that surface changes manifest themselves on a time scale of several hundred seconds.

Moreover, the upward trend of the relaxation time over the course of deposition time quantifies the slowing down process during the growth. However, it is not easy to establish a direct relationship between this time scale and specific processes. To find spatial correlations in our XPCS data and account for the heterogeneous behavior, we turn to simulations.

5. Simulations

To create a sufficiently large surface in real space and at the same time keep the computational costs low, it is possible to use effective theories, in particular the phase field theory, following the model in work [27], or construct a surface using kinetic Monte Carlo simulations [19]. Both simulations produce a model of a film surface consisting of rectangular pixels (see supplementary information figure S7(c)). This model includes the opening and closing of layers, and the formation and growth of islands, including coalescence. During surface change, we simulate the scattering process using the software BornAgain [28]. We can generate a coherent detector image for each time step by remaining within one layer using one particle layout. Finally, we calculate the TTC (equation (1)) from the simulated scattering data, using the same procedure as for the experimental data. The simulation can successfully reproduce the experimental data (figures 4(a) and (b)).

During the later growth phase, after the growth of the first two MLs, we focus on the evolution of islands. To achieve this, we can increase the resolution in real space by using cylinders with increasing radius and height to represent island growth [14]. With this method, we can not only capture the growth of individual islands, but also separate island growth from island movement. This distinction becomes particularly relevant during this growth phase, in contrast to the deposition of the first two MLs where we focus on the development of individual layers.

Since we maintain a constant material flow, we expect the volume of the islands to grow linearly. To achieve this, we vary the radius (and height) of the cylinders according to

$$r\left(t_{\text{dep}}\right) = r_0 + r_s \cdot t_{\text{dep}}^{1/3}, \tag{5}$$

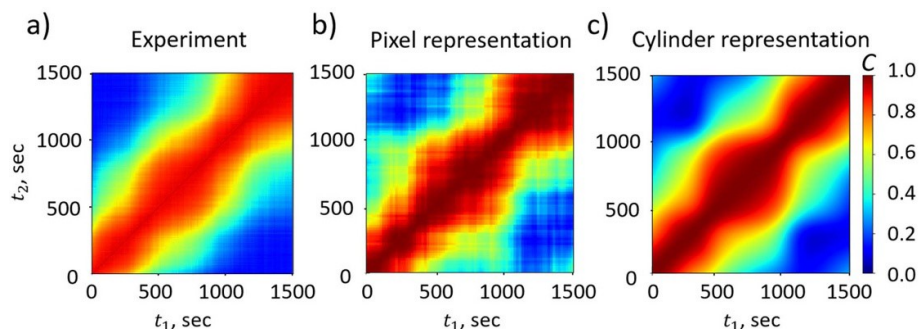**Figure 4.** (a) Experimental data from the intermediate growth scan ($t_{dep} = 2100$–3600 s in figure 2(b)). This scan covers the transition from layer-by-layer growth to islanding, where molecules assemble into 3D islands, growing in height and width over time. (b) Simulated TTC, generated from pixel real space. In the early growth phase we focus on the layer evolution. (c) Simulated TTC, generated from a surface with cylinders. This improves the resolution and allows separation of growth and movement during the later growth phase.
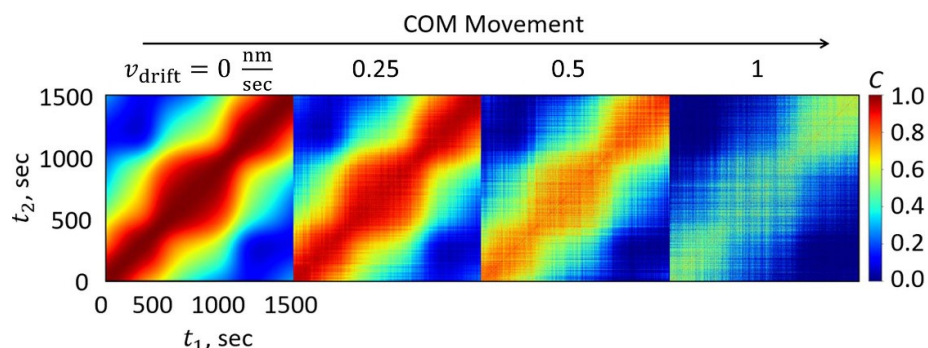
Figure 5. Investigation of the center of mass (COM) movement of the islands in the later growth phase. As the dynamics of the cylinders increase, indicated by the effective drift velocity v_{drift}, the TTC shape seen in the data is suppressed by the shape formed from the movement.

where r_0 is the initial radius and r_s is a scaling factor. The parameters are selected so that the simulation matches the data as closely as possible, using atomic force microscope (AFM) images (see supplementary information figure S4) and correlation lengths (figure 2(a)) as reference values. We randomly distribute 50 cylinders over an area of $10 \times 10\,\mu m^2$, taking care to avoid overlapping cylinders. The simulation results are shown in figure 4(c), focusing on the intermediate scan where the layer-by-layer transition to island growth occurs. Both representations (figures 4(b) and (c)) in real space give reliable results at this transition point, indicating the accuracy of the simulations compared to the experimental data.

Using the cylinder representation, we can focus on the movement of the islands during the later growth phase. To analyze this, we introduce a center of mass (COM) motion to each growth step of the cylinders in the simulation. The step spacing is chosen according to a normal distribution whose width is set proportional to the change in radius (extracted from equation (5)). To vary the dynamics, the step spacing is multiplied by several integers, leading to average effective drift velocities of about $v_{drift} = 0, 0.25, 0.5,$ and $1\,nm\,s^{-1}$, the resulting TTCs are shown in figure 5 (the effective drift velocity is defined by the total COM displacement per time). As the dynamics of the cylinders increase, the TTC shape from growth competes with the shape formed from motion. Comparing these results with the TTC shapes observed in the experimental data, we can roughly extract an average effective drift velocity of about $0.25\,nm\,s^{-1}$. This allows us to conclude that the changes in the coherent diffraction patterns, revealed by the analysis of the TTCs, arise predominantly from the growth of the islands while their movement has only a minor effect.

6. Heterogeneity analysis

Moving on to an analysis of the growth kinetics, we will take a closer look at the heterogeneous behavior of the TTCs, which is a crucial feature to consider. The growth kinetics can be analyzed by calculating the fourth order correlation function, given by [5, 29, 30]
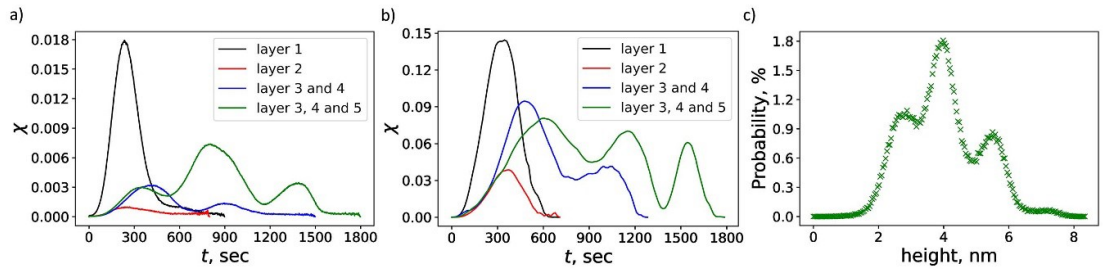
Figure 6. (a) Fourth order correlation functions obtained from experimental data using equation (6). Different lines correspond to the growth of different layers: black—growth and closure of layer 1 ($t_{dep} = 100$–1000 s), red—growth and closure of layer 2 ($t_{dep} = 1000$–1800 s), blue—simultaneously overlapping growth of layers 3 and 4 ($t_{dep} = 2100$–3600 s), green—growth of layers 3, 4 and 5 ($t_{dep} = 3600$–5400 s). (b) Simulated fourth order correlation functions obtained from the pixel representation and calculated using the same procedure as for the experimental data. (c) Height distribution function of a 10 nm DIP film grown under the same conditions, obtained from atomic force microscopy measurements after the film growth. The peaks correspond to open layers.

$$\chi(\mathbf{q}, t) = \frac{\langle C(\mathbf{q}, t_1, t)^2 \rangle_{t_1} - \langle C(\mathbf{q}, t_1, t) \rangle_{t_1}^2}{\langle C(\mathbf{q}, t_1, t = 0) \rangle_{t_1}^2}, \tag{6}$$

with t being defined in equation (3). The resulting graphs typically show a peak at a position t^*, which corresponds to the characteristic time of the system, with a height χ^*, indicating the degree of heterogeneity.

For the calculation of the experimental data, we extract the heterogeneity function for the first two layers separately (layer 1: $t_{dep} = 100$–1000 s, layer 2: $t_{dep} = 1000$–1800 s), to have better access to the evolution of the separate layers in the beginning. Subsequently, we analyze the roughening of the film (starting from layer 3), shown in figure 6(a). To understand the meaning of the occurrence of several peaks and the position and height of each individual peak, we compare the results to the simulation.

The appearance of heterogeneous dynamics can be explained by the opening and closing of layers, as described in [10]. However, the simulation shows that a similar effect can be obtained by pure island (cylinder) growth, which fits to the occurrence of heterogeneous behavior when the layers no longer close completely (starting from the 3rd layer). As the cylinders grow, intensity peaks of the form factor shift on the detector, creating 'irregularities' along the main diagonal of the TTC (compare with [31]), which results in the appearance of successive peaks of the fourth order correlation function $\chi(t)$. As the size distribution of the domains increases, the peaks become less distinct, revealing information about the roughness of the surface (see supplementary information figure S5). Therefore, a decrease in the peak height (χ^*) observed in the fourth order correlation function corresponds to an increase in surface roughness.

In the following, we investigate the occurrence of multiple heterogeneity peaks. According to the definition of the fourth order correlation function in equation (6), $\chi(t) \neq 0$ results if at a certain time $t = |t_2 - t_1|$ there is some change along the diagonal. If at a later time $t' > t$ the diagonal remains unchanged, this leads to $\chi(t') = 0$. A subsequent change at some $t'' > t'$ leads again to $\chi(t'') \neq 0$. This either happens for well-separated off-diagonal elements or for alternating oscillations along the diagonal. We observe that the latter arises from the mixing of intensity peaks originating from different characteristic sizes in the cylinder representation (compare with figure 4). This mixing occurs due to the interaction between the growth of the radius and the change in height, which in general can also be applied to the interference between multiple radii or heights that intermix with each other. From the evolution of the correlation peaks (as seen in figure 2(a)), we expect that the radius does not change dramatically, so we can translate different sizes into characteristic heights on the surface. Generalizing this result we make the assumption that several heterogeneity peaks correspond to the opening of layers (different heights) on the surface. Therefore, each peak at t^* represents the characteristic time at which the corresponding layer coverage evolves. We discover the same for the pixel representation, where the number of open layers corresponds to the number of peaks in the fourth order correlation function. Based on these findings, we can simulate a growth behavior using the pixel representation that results in a heterogeneity structure very similar to that observed in the experimental data, shown in figure 6(b).

As a result, we can now utilize these insights to interpret the experimental data. In these, t^* increases during growth, indicating that the growth process slows down during the deposition time, especially when several layers evolve simultaneously. This is a physically reasonable result in terms of the constant flow of material being divided between several layers. At the same time, χ^* decreases after the first layer, indicating that the size distribution of the islands (i.e. roughness) increases with deposition time. While only one layer is formed (layers 1 and 2), the heterogeneity calculation results in a single peak. This trend seems to persist to

some extent even when the film undergoes a transition to a rougher state, reflecting the simultaneous evolution of the layers by the number of peaks in the fourth order correlation function. Accordingly, the function subsequently splits into two peaks, indicating that the growth of layers 3 and 4 overlap. At the end of the growth, we observe three peaks, which can be translated into three open layers. Comparing the final statement with the AFM data of a DIP film grown under the same conditions, the height profile confirms this assumption, as shown in figure 6(c).

7. Conclusions

In conclusion, the XPCS analysis allows to study the complex growth process of thin films, especially the growth and movement of island structures on the surface. The calculation of the two-time correlation function revealed a striking heterogeneous behavior and revealed time scales of surface changes in the range of several hundred seconds using a conventional g_2 analysis.

Furthermore, we can attribute the TTC shape to kinetic effects, suggesting an approximately static evolution of the islands. A more detailed comparison revealed that the heterogeneity appears not only due to the opening and closing of layers, but also due to the growth of the islands. To quantify this further, we calculated the fourth order correlation function. We were able to translate the number of peaks in the fourth order correlation function into the number of open layers on the surface. In addition, the height and position of each peak corresponds to the roughness and speed of the individual layer evolution, respectively. The experimental findings are supported by numerical simulations.

The analysis allows to characterize layer-by-layer growth and pinpoint the transition to islanding, which leads to a roughening of the film. Even in this latter regime, the number of peaks in the fourth order correlation function can be attributed to the number of open layers. Our approach can be applied rather generally to other materials and also the impact of external parameters to understand the microscopic dynamics underlying structure formation.

Data availability statement

All data that support the findings of this study are included within the article (and any supplementary files).

Acknowledgments

ORCID iDs

I A Zaluzhnyy ⓘ https://orcid.org/0000-0001-5946-2777
V Starostin ⓘ https://orcid.org/0000-0003-4533-6256
R Rysov ⓘ https://orcid.org/0000-0002-7589-0808
F Westermeier ⓘ https://orcid.org/0000-0003-0696-206X
L Pithan ⓘ https://orcid.org/0000-0002-6080-3273
F Schreiber ⓘ https://orcid.org/0000-0003-3659-6718

References

[1] Oura K, Katayama M, Zotov A V, Lifshits V G and Saranin A A 2003 Growth of thin films *Advanced Texts in Physics* (Springer) pp 357–87
[2] Krug J 1997 *Adv. Phys.* **46** 139–282
[3] Seeck O H and Murphy B (eds) 2015 *X-Ray Diffraction* (Jenny Stanford Publishing)
[4] Shpyrko O G 2014 *J. Synchrotron Radiat.* **21** 1057–64
[5] Sinha S K, Jiang Z and Lurio L B 2014 *Adv. Mater.* **26** 7764–85
[6] Madsen A, Leheny R L, Guo H, Sprung M and Czakkel O 2010 *New J. Phys.* **12** 055001
[7] Madsen A, Fluerasu A and Ruta B 2016 Structural dynamics of materials probed by x-ray photon correlation spectroscopy *Synchrotron Light Sources and Free-Electron Lasers* (Springer) pp 1617–41
[8] Madsen A, Seydel T, Sprung M, Gutt C, Tolan M and Grübel G 2004 *Phys. Rev. Lett.* **92** 096104
[9] Gutt C, Ghaderi T, Tolan M, Sinha S K and Grübel G 2008 *Phys. Rev.* B **77** 094133

[10] Ju G, Xu D, Highland M J, Thompson C, Zhou H, Eastman J A, Fuoss P H, Zapol P, Kim H and Stephenson G B 2019 *Nat. Phys.* **15** 589–94

[11] Headrick R, Ulbrandt J, Myint P, Wan J, Li Y, Fluerasu A, Zhang Y, Wiegart L and Ludwig K 2019 *Nat. Commun.* **10** 2638

[12] Dürr A C, Schreiber F, Ritley K A, Kruppa V, Krug J, Dosch H and Struth B 2003 *Phys. Rev. Lett.* **90** 016104

[13] Kowarik S, Gerlach A, Sellner S, Schreiber F, Cavalcanti L and Konovalov O 2006 *Phys. Rev. Lett.* **96** 125504

[14] Frank C, Banerjee R, Oettel M, Gerlach A, Novák J, Santoro G and Schreiber F 2014 *Phys. Rev. B* **90** 205401

[15] Schreiber F 2004 *Phys. Status Solidi* a **201** 1037–54

[16] Ruiz R, Nickel B, Koch N, Feldman L C, Haglund R F, Kahn A, Family F and Scoles G 2003 *Phys. Rev. Lett.* **91** 136102

[17] Lorini E, Soprani L and Muccioli L 2023 *Adv. Theory Simul.* **6** 2300080

[18] Käfer D, Ruppel L, Witte G and Wöll C 2005 *Phys. Rev. Lett.* **95** 166602

[19] Empting E, Bader N and Oettel M 2022 *Phys. Rev. E* **105** 045306

[20] Frank C, Novák J, Banerjee R, Gerlach A, Schreiber F, Vorobiev A and Kowarik S 2014 *Phys. Rev. B* **90** 045410

[21] Ritley K A, Krause B, Schreiber F and Dosch H 2001 *Rev. Sci. Instrum.* **72** 1453–7

[22] Renaud G, Lazzari R and Leroy F 2009 *Surf. Sci. Rep.* **64** 255–380

[23] Bommel S, Kleppmann N, Weber C, Spranger H, Schäfer P, Novák J, Roth S, Schreiber F, Klapp S and Kowarik S 2014 *Nat. Commun.* **5** 5388

[24] Sinha S K, Sirota E B, Garoff S and Stanley H B 1988 *Phys. Rev. B* **38** 2297–311

[25] Bikondoa O 2017 *J. Appl. Crystallogr.* **50** 357–68

[26] Begam N *et al* 2021 *Phys. Rev. Lett.* **126** 098001

[27] Yu Y-M and Liu B-G 2004 *Phys. Rev. E* **69** 021601

[28] Pospelov G, Van Herck W, Burle J, Carmona Loaiza J M, Durniak C, Fisher J M, Ganeva M, Yurov D and Wuttke J 2020 *J. Appl. Crystallogr.* **53** 262–76

[29] Berthier L, Biroli G, Bouchaud J-P, Cipelletti L, Masri D E, L'Hôte D, Ladieu F and Pierno M 2005 *Science* **310** 1797–800

[30] Berthier L 2011 *Physics* **4** 42

[31] Ragulskaya A *et al* 2022 *IUCrJ* **9** 439–48